Surface phonons of the Si(111)-(7×7) reconstruction observed by Raman spectroscopy

M. Liebhaber,[1] U. Bass,[1] P. Bayersdorfer,[2] and J. Geurts[1,*]
[1]*Universität Würzburg, Physikalisches Institut, Experimental Physics 3, Am Hubland, 97074 Würzburg, Germany*
[2]*Universität Würzburg, Physikalisches Institut, Experimental Physics 7, Am Hubland, 97074 Würzburg, Germany*

E. Speiser, J. Räthel, A. Baumann, S. Chandola, and N. Esser
Leibniz-Institut für Analytische Wissenschaften - ISAS - e.V., Albert-Einstein-Strasse 9, 12489 Berlin, Germany
(Received 14 October 2013; revised manuscript received 26 November 2013; published 29 January 2014)

We have studied the surface phonon modes of the reconstructed Si(111)-(7×7) surface by polarized Raman spectroscopy. Six surface vibration modes are observed in the frequency range between 62.5 and 420.0 cm^{-1}. The mode frequencies agree very well with reported calculation results. This enables their attribution to calculated eigenmodes, whose elongation patterns are dominated by specific atomic sites: the two most characteristic novel fingerprints of the (7×7) reconstruction are sharp Raman peaks from localized adatom vibrations, located at 250.9 cm^{-1}, and collective vibrations of the adatoms and first- and second-layer atoms, located at 420.0 cm^{-1}. While the sharp localized adatom vibration peak is a substantial refinement of an earlier broad spectral structure from electron energy-loss spectroscopy, no spectroscopic features were reported before in the collective-vibration frequency region. Furthermore, we observe in-plane wagging vibrations in the range from 110 to 140 cm^{-1}, and finally the backfolded acoustic Rayleigh wave at 62.5 cm^{-1}, which coincides with helium atom scattering data. Moreover, the Raman peak intensities of the surface phonons show a mode-specific dependence on the polarization directions of incident and scattered light. From this polarization dependence the relevant symmetry components in the Raman scattering process (A_1 and/or E symmetry) are deduced for each mode.

DOI: 10.1103/PhysRevB.89.045313 PACS number(s): 78.30.Am, 68.47.Fg, 68.35.bg, 68.35.Ja

I. INTRODUCTION

The (7×7) reconstruction of the Si(111) surface is probably one of the most complex and widely studied solid surfaces. Since its first observation by low-energy electron diffraction (LEED) [1], considerable experimental and theoretical research effort has been spent to clarify the atomic arrangement of this surface (for a survey, see, e.g., [2,3]). Scanning tunneling microscopy (STM) allowed a first real-space image of the (7×7) surface [4]. Takayanagi *et al*. [5] established the famous *dimer-adatom-stacking fault* (DAS) structural model by including the evaluation of the spot intensity distributions of transmission electron diffraction (TED) data. The DAS model is generally accepted as the correct description of the surface atomic structure. It is in excellent agreement with all available experimental results, e.g., dynamical LEED analysis [6], STM [4,7], and high-resolution transmission electron microscopy (HRTEM) imaging [8], angle-resolved photoemission spectroscopy (ARPES) [9–11], and x-ray diffraction XRD [12]. In addition, several theoretical calculations on the Si(111)-(7×7) surface relaxation have confirmed the DAS geometry and proved that this is the energetically favorable Si(111) surface reconstruction [13–15]. The structural model is described in detail in Sec. II.

This paper will focus on the dynamical properties of the Si(111)-(7×7) surface structure. In general, the vibronic spectrum of a solid surface is expected to differ from its bulk phonon dispersion relation due to lower dimensionality, different atomic structure, and altered chemical bonding [16,17]. Intrinsically surface-sensitive techniques, such as high-resolution electron energy-loss spectroscopy (HREELS) [18–20] and helium atom scattering (HAS) [21,22], are the well-established experimental tools for analyzing surface lattice vibrations. In recent years, also Raman spectroscopy (RS) as an optical technique, traditionally widely used for investigating phonons in semiconductor bulk and multilayers, has been successfully applied to probe surface vibration modes of clean surfaces as well as ordered adsorbed (sub)monolayers [16,17,23–28]. This development was facilitated by resonant enhancement of the excitation and by the enormous improvement of detection sensitivity. The Raman intensity of surface phonons is expected to be far below the bulk scattering intensity, because the scattering volume of the surface vibration modes is confined to the topmost atomic layers and is thus much smaller than the bulk scattering region, which is determined by the penetration depth of light, above 100 Å up to infinite, depending on the photon energy [16,17]. When comparing HREELS, HAS, and RS, we note important implications of their different probing particles (electrons, atoms, and photons, respectively) and scattering mechanisms. HREELS and HAS imply certain limitations concerning spectral range, spectral resolution, and phonon symmetry selection rules but allow the determination of the full surface phonon dispersion. RS, in contrast, which depends on the photon-phonon interaction, is limited to Brillouin zone (BZ) center phonon excitations. It should be noted that this zone center limitation only applies for one-phonon scattering. However, if two-phonon processes are considered, this limitation is lifted and according to the momentum conservation law, all phonon states may contribute to the Raman spectrum such that the sum of their momenta must be approximately zero [29]. The major advantage of RS is its high spectral resolution in the range of 1 cm^{-1}, which is significantly better than that of HREELS

*geurts@physik.uni-wuerzburg.de

(approx. 10 cm^{-1} [30]), over a wide range of phonon energies. In addition, with defined light polarization configurations, Raman scattering also reveals surface phonon symmetry properties.

In this paper we report on the observation of surface phonon modes of the Si(111)-(7×7) surface reconstruction resolved by RS and compare our results to various theoretical modeling studies [31–34] and existing experimental data of the complementary methods, i.e., HREELS [35] and HAS [36].

As a basic requirement for the surface vibration mode assignment, the paper starts with a discussion of the DAS surface atomic arrangement, followed by its symmetry considerations, which are reflected in the Raman tensors. After a survey of the sample preparation procedure and the experimental setup, the results are presented. In our experiments we employed LEED as a quality criterion for the surface preparation. Subsequently, for the Raman spectra, the distinction between the net surface signatures and the very intense background from bulk contributions is addressed. Finally, the obtained surface Raman signatures are discussed, and a mode assignment in terms of local vibrations of the adatoms, their collective vibrations with the first- and second-layer atoms, in-plane wagging vibrations, and the backfolded acoustic Rayleigh wave is performed in accordance with model calculations of different theoretical methods.

II. ATOMIC ARRANGEMENT AND SYMMETRY OF THE Si(111)-(7×7) SURFACE

For a comprehensive interpretation of the surface phonon modes, the detailed atomic arrangement of the Si(111)-(7×7) reconstructed surface must be considered. As described in the DAS model [5], the reduction of the number of dangling bonds is achieved by a rigorous atomic rearrangement. Figure 1 illustrates the DAS rhomboidal surface unit cell, which consists of a pair of triangular subcells with different stacking sequences (faulted and unfaulted halves) and dimerization along these cell boundaries. There are three classes of atoms remaining with dangling bonds: (i) each surface unit cell has 12 *adatoms* in the topmost Si layer, labeled as layer 0 in Fig. 1(b). They are arranged in triangles. Six of them occupy the corner sites (indicated with a C), and the other six occupy the edge center sites (indicated with an E). (ii) The first (semi-)complete Si layer, denoted as layer 1, incorporates in each unit cell six *rest atoms* (marked with a +sign), and (iii) layer 3 contains one unsaturated *corner hole atom*. Thus the number of dangling bonds pointing to the vacuum is reduced from formerly 49 for the unreconstructed Si(111) surface to $12 + 6 + 1 = 19$ in the (7×7) reconstructed surface unit cell. Layer 1 also contains triples of saturated *backbone atoms*, acting as bonds to the adatoms. In addition, this complex atomic arrangement is expected to give rise to a rich variety of surface vibration modes with mode-specific participation of the various atomic sites and the corresponding bond orbitals. In RS, this should lead to vibration frequencies in a broad spectral range.

RS experiments with defined polarization directions e_i and e_s of the electronic fields of the incoming and scattered light not only give access to the vibration mode frequencies,

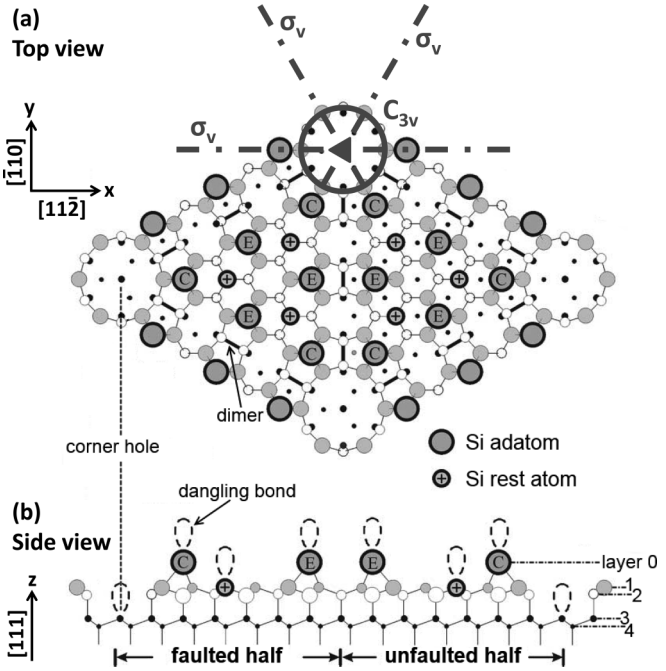

FIG. 1. (a) Top view of the DAS geometry of the Si(111)-(7×7) reconstructed surface by Takayanagi *et al.* [5]. The rhomboidal surface unit cells consist of faulted and unfaulted half cells, separated by rows of dimers (full black lines, connecting neighbor atoms). Each half cell contains six adatoms (layer 0), arranged in a triangle: three at its corner sites (indicated with a C), the other three at its edge center sites (indicated with an E). The Si rest atoms in layer 1 are marked with + signs. The gray dash-dotted lines and the triangle and circle symbols indicate the C_{3v} surface symmetry. (b) Side view with visualization of the dangling bonds and numbering of the surface layers. (Figure adapted from Ref. [37].)

but also may reveal their symmetries. For all irreducible representations of the crystallographic point groups, the symmetry-induced selection rules are given as Raman tensors [38], tabulated, e.g., in Ref. [29]. Bulk Si, which crystalizes in the diamond structure, belongs to the point group O_h ($m3m$). For Raman backscattering from the (111) surface, the principal in-plane axes for light polarization are the [11$\bar{2}$] and [$\bar{1}$10] crystal directions.

For the rhomboidal (7×7) surface unit cell, after the reconstruction-imposed symmetry reduction, a threefold axis of symmetry (C_3) and reflections on three vertical mirror planes (σ_v) remain, as depicted in Fig. 1(a). Thus it belongs to the point group C_{3v} ($3m$) [39]. For this group, the Raman-active phonon modes have A_1 and E symmetry. The A_1 modes give rise to polarized scattering, i.e., the polarization direction e_s of the outgoing Raman light is parallel to the polarization direction e_i of the incoming laser light. For the E modes the scattering is depolarized, which results in Raman light with polarization direction e_s perpendicular to the incoming e_i [29,39]. When denoting the threefold rotation axis normal to the surface as z, and the in-plane axes as x and y, for deformation potential Raman scattering in backscattering geometry the diagonal Raman tensor elements xx and yy are relevant for A_1 modes and the off-diagonal elements xy and yx for E modes [29,39]. The connection of the directions

x, y, and z of this surface coordinate system to the Si bulk axes is given by $x = [11\bar{2}]$, $y = [\bar{1}10]$, and $z = [111]$. In the well-established Porto notation [29,40], backscattering from a z-oriented surface with incoming and outgoing polarization directions e_i and e_s, respectively, is denoted as $z(e_i e_s)\bar{z}$. Following this notation, A_1 modes only appear in the parallel polarization configurations $z(xx)\bar{z}$ and $z(yy)\bar{z}$ (= polarized), while the E modes are expected to appear in the perpendicular polarization configurations $z(xy)\bar{z}$ and $z(yx)\bar{z}$ (= depolarized) [29,39]. For a specific C_{3v} system, the actual number of A and E modes is governed by the number of atoms in its unit cell. Thus, for the Si(111)-(7×7) surface, a very high number of vibration modes may be expected. This subject will be discussed in detail in Sec. IV C, in which the experimentally observed Raman peaks are assigned to calculated surface vibration eigenmodes.

III. EXPERIMENT

The experiments were performed on samples from commercially available Si(111) wafers with a feasibly small miscut angle below 0.5°. Doping was n type (dopant Sb, $\rho < 0.01$ Ω cm) and p type (dopant B, $\rho \approx 0.1$–1 Ω cm), respectively. For the preparation of the (7×7) surface reconstruction, the samples were initially pretreated in an *ex situ* wet-chemical cleaning procedure, followed by an *in situ* flash annealing process. In detail, they were first cleaned in an ultrasonic bath with acetone and isopropanol and subsequently immediately transferred into the UHV system with a base pressure below 2×10^{-10} mbar. There, degassing was performed for 8 h at 700 °C, followed by flashing at a temperature of approx. 1200 °C for only a few seconds while keeping the pressure below 1×10^{-9} mbar. Thereafter, a rapid cooldown to 900 °C followed by a slow cooling to room temperature (RT) delivers the best results. If required, this flash annealing process was repeated several times until a clean (7×7) surface was obtained. For monitoring the surface quality, LEED was employed in between. The quality of the applied surface preparation procedure is underscored by quantitative electron diffraction spot profile analysis in concomitant SPA-LEED experiments, yielding a very narrow peak width of 0.065 nm^{-1} under in-phase scattering conditions, which is limited instrumentally by the SPA-LEED coherence length of 90 nm.

To study surface vibration modes, *in situ* RS was performed using a spectroscopy setup in near-backscattering geometry which was directly attached to the UHV system. To validate the reproducibility and exclude setup artifacts, these Raman measurements were performed twice, using two different setups with distinct high-sensitivity spectrometer types, a triple DILOR-XY and a SPEX 1403 double monochromator, both with an efficient rejection of the elastically scattered laser light and equipped with high-efficiency Si-based CCD detectors (ANDOR iDus series). In order to verify the Raman origin of the observed spectral features (i.e., exclusion of photoluminescence) and to check for possible resonance effects, the excitation energy was varied between 2.54 and 2.41 eV, the 488- and 514-nm laser line of an Ar^+-ion laser, respectively. Besides these two lines, the 532-nm laser line (photon energy 2.33 eV) of a Nd:YAG laser was also employed. To exclude temperature effects the lasers were operated at moderate power below 130 mW (focus diameter ∼50–100 μm). For low-temperature (LT) measurements, sample cooling was achieved by a closed-cycle helium cryostat.

IV. RESULTS AND DISCUSSION

A. LEED analysis

Figure 2 shows the LEED pattern obtained at 300 K, with an electron energy of 38 eV from the (7×7)-reconstructed Si(111) surface, prepared by the flash annealing process described above. The high-quality (7×7) surface periodicity in real space is reflected in the six sharp extra spots in between the (1×1) main diffraction spots (circled in Fig. 2). Furthermore, the pattern shows the threefold symmetry of this C_{3v}-type reconstruction. Besides the quality check of the surface, LEED also allowed the identification of the in-plane crystal directions ($[11\bar{2}]$ and $[\bar{1}10]$) as a reference for polarized RS.

B. UHV Raman spectra

In this section the experimentally observed surface phonon modes of the Si(111)-(7×7) reconstruction are presented in detail. For identifying these modes, RT Raman spectra with an excitation energy of 2.41 eV were recorded *in situ* in UHV, immediately after the flash annealing preparation of the clean (7×7) reconstructed surface, and for comparison subsequently also after accelerated aging of the surface by exposure to an increased base pressure of the residual gas ($p \approx 10^{-8}$ mbar) for more than 10 min. For these experiments n-type Si samples were used.

Because RS is not an intrinsically surface-sensitive technique, surface phonon Raman spectra are always a superposition of the generally comparably weak surface vibration contributions and an intense bulk signal. This is confirmed in the Raman spectrum of Si(111)-(7×7), shown in Fig. 3(a). Its dominant feature, located at 520.7 cm^{-1} and exceeding by far (∼ factor 40) the intensity scale, originates from first-order Raman scattering from the bulk Si phonon, with

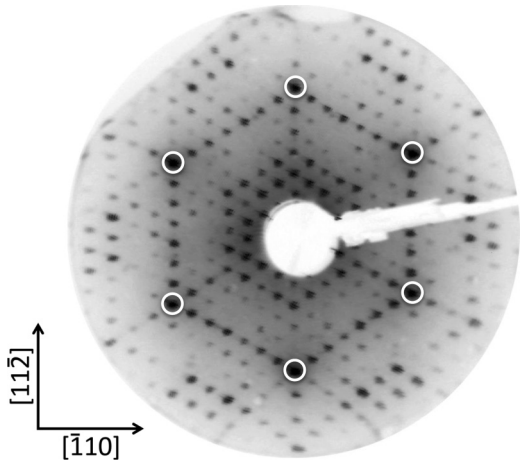

FIG. 2. LEED pattern of a reconstructed Si(111)-(7×7) surface at 300 K, taken with an electron energy of 38 eV, showing the crystal superstructure and the orientation of the in-plane crystal axes $[11\bar{2}]$ and $[\bar{1}10]$.

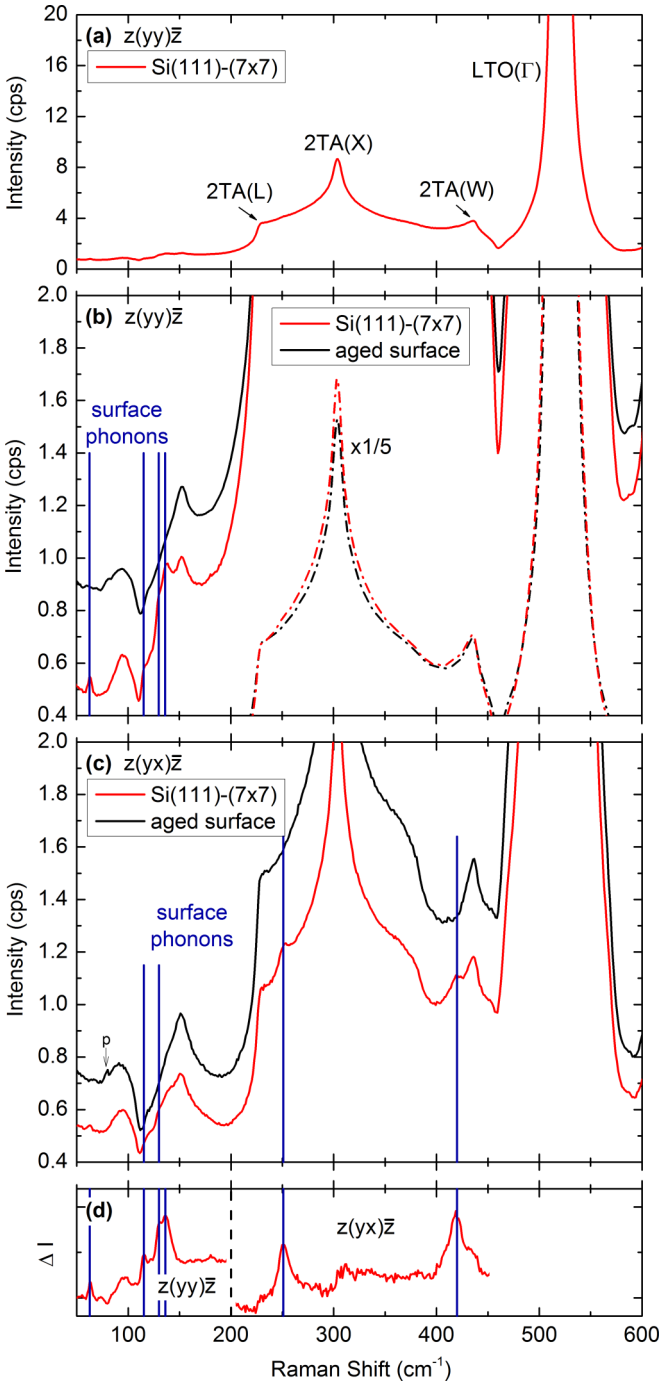

FIG. 3. (Color online) Raman spectra of Si(111) at 300 K, excitation 2.41 eV. (a) (7×7) surface, polarization configuration z(yy)z̄; intensity scaling adapted for bulk two-phonon signatures cutting off the one-phonon LTO(Γ) peak. (b, c) Freshly prepared Si(111)-(7×7) surface (red curves) and after aging (black curves, vertically shifted). Configurations: z(yy)z̄ for (b) and z(yx)z̄ for (c). The additional intensity zoom factor of 10 allows the observation of six phonon modes from the (7×7) surface, marked by vertical blue lines, which are totally quenched upon aging. (Note: Peak p, at 78 cm^{-1}, is a plasma line.) (d) Intensity difference between the (7×7) surface and the aged one illustrating the essential surface vibrations: up to 200 cm^{-1} the configuration z(yy)z̄ is shown, and z(yx)z̄ from 200 to 450 cm^{-1}.

a wave vector close to the BZ center (Γ point). Because of the nonpolar bonding of Si, the transverse optical (TO) and longitudinal optical (LO) phonon branch are degenerate in this region of the BZ [29]. Therefore this peak is denoted in the following as LTO(Γ). This sharp and intense one-phonon Raman peak is accompanied by the broadly structured second-order vibrational Raman signature with much lower (approx. 10^{-2}) intensity. Its most prominent structure is a clear peak at 303 cm^{-1}, originating from 2TA at the *X* point of the BZ. Furthermore, edgelike structures at 230 and 435 cm^{-1} arise from 2TA at the L and W point, respectively [41–43].

On this intensity scale, surface peaks cannot yet be distinguished due to their very weak scattering intensity. Their extraction requires a strong intensity zoom. Figures 3(b) and 3(c) show the Raman spectra with an additional intensity upscaling by a factor of 10 as compared to Fig. 3(a).

This allows the extraction of features as weak as $\sim 10^{-4}$ × the LTO(Γ)-mode intensity. The spectra of Fig. 3(b) were recorded in a parallel polarization configuration, aligned on the $y = [\bar{1}10]$ in-plane sample axis (as depicted in Fig. 1), i.e., z(yy)z̄ in the Porto notation. For comparison, spectra in perpendicular polarization configuration z(yx)z̄ are shown in Fig. 3(c). The red curves belong to the clean (7×7) reconstructed surface immediately after the flash-annealing preparation; the black ones originate from the subsequently aged (i.e., gas-exposed) surface, after the extinction of the (7×7) reconstruction.

In the spectra of the reconstructed (7×7) surface, besides the second-order features from bulk Si discussed above, additional low-intensity peaks appear, located at 62.5, 136.1, 250.9, and 420.0 cm^{-1}, and indications of new features in the range between 110 and 140 cm^{-1}. They are marked by the blue vertical lines in Figs. 3(b) and 3(c). After accelerated aging they have completely disappeared, which is clear evidence for their classification as surface phonon modes induced by the (7×7) reconstruction. The low surface phonon intensity indicates that we deal with off-resonant Raman scattering, in contrast to, e.g., In/Si(111) [25,26]. For clarification, the net contributions of the prominent surface vibration peaks are presented in Fig. 3(d), which shows the intensity difference between the (7×7) reconstructed surface and the aged one. In order to focus on the essential peaks, the spectral range up to 200 cm^{-1} is shown for the z(yy)z̄ configuration and the range between 200 and 450 cm^{-1} for the z(yx)z̄ configuration.

Moreover, polarization dependencies are observed for four out of the six detected surface phonon modes. The dominant polarization configuration for the two modes at 62.5 cm^{-1} and 136.1 cm^{-1} is z(yy)z̄, i.e., parallel, and for the higher frequency modes at 250.9 cm^{-1} and 420.0 cm^{-1} z(yx)z̄, i.e., crossed.

For an unambiguous identification of the surface-related peaks located in the edgelike two-phonon structure between 110 and 150 cm^{-1}, LT Raman measurements were performed at 40 K. Figure 4 shows the spectra of the clean Si(111)-(7×7) reconstructed surface in parallel z(yy)z̄ and crossed z(yx)z̄ polarization configurations. In these measurements, the three surface phonon modes at 115.3, 130.0, and 136.1 cm^{-1} are better resolved, because the two-phonon edgelike structure is significantly suppressed. This is a result of the reduced Bose-Einstein factor $n(\omega, T)$. The T dependence of the intensity

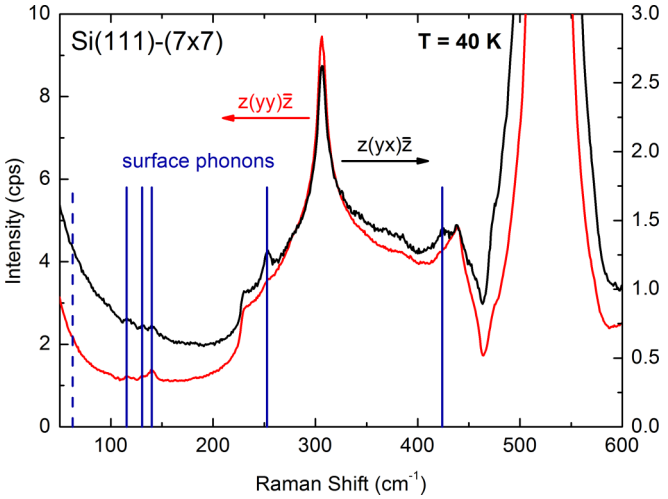

FIG. 4. (Color online) LT Raman spectra of the clean Si(111)-(7×7) surface in parallel z(yy)z̄ (red) and crossed z(yx)z̄ (black) polarization configurations, recorded at 40 K with an excitation energy of 2.33 eV. At LT, the three surface phonons at 115.3, 130.0, and 136.1 cm^{-1}, respectively, are better resolved because of the significant suppression of the two-phonon edgelike structure (arising between 110 and 150 cm^{-1} for RT). In the frequency range below 100 cm^{-1} the surface phonon observation is hampered by the high-intensity tail of the elastically scattered laser light.

for second-order scattering is much more pronounced than for first-order scattering processes, since the first-order intensity at a certain frequency ω is proportional to $[n(\omega,T)+1]$, while for second-order processes the square of $[n(\omega/2,T)+1]$ applies [29,44]. In the spectral range below 100 cm^{-1}, the detection of low-intensity surface phonon modes is hampered by the high-intensity tail of the elastically scattered laser light. The LT spectra were recorded with a different excitation energy of 2.33 eV and a differently doped (p-type) Si sample. The application of different laser energies allows to check for resonance effects in the Raman scattering efficiency. Here, the 2.33-eV excitation yields surface phonon peak intensities comparable to those from the 2.41-eV excitation (Fig. 3). The same applies for data from 2.54-eV excitation (not shown). Thus no resonance effects were observed. However, as the Raman shifts of the modes are independent of the applied laser line, this is a conclusive proof of their origin from inelastic light scattering. Moreover, their identical occurrence for differently doped samples manifests the evidence that the detected surface phonons are intrinsically representative for the reconstructed (7×7) surface and are not caused by vibrations of diffused dopant atoms at the surface.

A further evidence for the assignment of the surface Raman peaks to vibration modes of the Si(111)-(7×7) reconstruction is their behavior upon submonolayer deposition of Au on the Si surface. In this case the peaks are quenched and replaced by new vibration modes, whose detailed behavior is governed by the Au reconstructions $(\sqrt{3}\times\sqrt{3})$ R30° or (5×2). They will be discussed elsewhere (unpublished).

The observed Si(111)-(7×7) surface phonon peak frequencies are summarized in Table I. For those peaks which predominantly occur in one polarization configuration, the corresponding Porto notation is included.

C. Surface phonon mode interpretation

The basis for the assignment of the observed surface Raman peaks to surface vibration eigenmodes of the Si(111)-(7×7) reconstruction is provided by various theoretical studies, which are briefly summarized in the following. For detailed information the reader is directly referred to Refs. [31–34]. It is important to emphasize that the extraordinarily large size of the reconstructed (7×7) surface unit cell constitutes a major challenge and requires high computational effort for all modeling studies. Kim *et al.* [31] and Štich *et al.* [32,33] apply molecular-dynamics (MD) simulations, based on the same supercell: a slab geometry which allows the relaxation of 151 unit-cell atoms that are located in layers 0–3 (Fig. 1). In Ref. [34] (Liu *et al.*), the next three layers are involved too. The MD calculations of Ref. [31] are based on the Car-Parrinello method. References [32,33] apply plane-wave pseudopotential techniques and a local-density approximation, while Ref. [34] relies on a nonorthogonal tight-binding Hamiltonian. The frequency spectrum can be obtained from the temporal evolution of the atomic elongation pattern by Fourier transform. The very high number of atoms gives rise to an extremely rich series of eigenmodes: 151 moving atoms induce 453 vibration eigenfrequencies, i.e., a quasicontinuous spectrum. However, all calculations yield a series of maxima of the envelope function, centered around several well-defined frequency values. These maxima are attributed to distinct elongation patterns, with specific participation of the various atomic species, e.g., the adatoms, backbone, or rest atoms. The

TABLE I. Summary of the surface phonon mode properties: frequencies at 300 K, preferential polarization configuration for Raman observation (if applicable), corresponding theoretically derived frequency range, mode assignment, and experimental observation by a different experimental technique (if applicable).

Raman position (cm^{-1})	Dominant polariz. config.	Theoretical results [31,33,34] frequency range (cm^{-1})	Mode assignment	Other experimental techniques
62.5	z(yy)z̄	60–100	Rayleigh wave	HAS [36]
115.3		110	In-plane wagging modes (adatom – atom underneath)	
130.0		–		
136.1	z(yy)z̄	140		
250.9	z(yx)z̄	220–280	Localized at adatomic sites	HREELS [35]
420.0	z(yx)z̄	400–460	Collective mode (adatoms, 1st- and 2nd-layer atoms)	

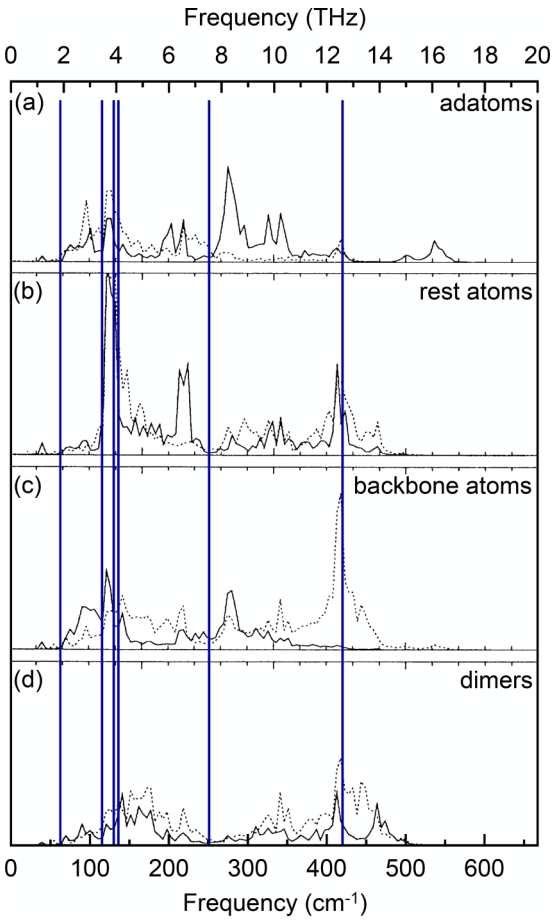

FIG. 5. (Color online) Calculated power spectra of the surface atom vibrations: (a) the adatoms, (b) the rest atoms, (c) the backbone atoms, and (d) the dimers. Solid curves: normal-to-plane displacement vector component; dotted curves: in-plane displacement vector component. (Figure adapted from Ref. [31].) The peak frequencies in the Raman spectra are marked by blue vertical lines.

various theoretical considerations in Refs. [31–34] give overall consistent results, although in detail some discrepancies occur. Depending on the calculation method, the resulting number of pronounced maxima is six to eight, with frequency values up to about 600 cm^{-1}. For illustration, Fig. 5 shows the calculated power spectra of the surface atom vibrations, adapted from Ref. [31]. In panels (a)–(d) the displacement contributions of the individual atomic sites are plotted: (a) the adatoms, (b) the rest atoms, (c) the backbone atoms, and (d) the dimers. The normal-to-plane and the in-plane components of the displacement vectors are shown separately as full and dotted curves, respectively. The most prominent features of the power spectra show a good correspondence to the experimental difference spectra of Fig. 3(d). In the following, the calculated frequencies of envelope maxima are compared with our experimentally determined Raman peak frequencies.

The spectral positions of all experimentally observed peaks coincide with calculated frequencies of maximum intensity, especially when taking into account the spectral spread between the results of the various calculation methods, indicated by the frequency intervals in Table I. When assigning them to specific eigenmodes, it must be noted that in the different calculations

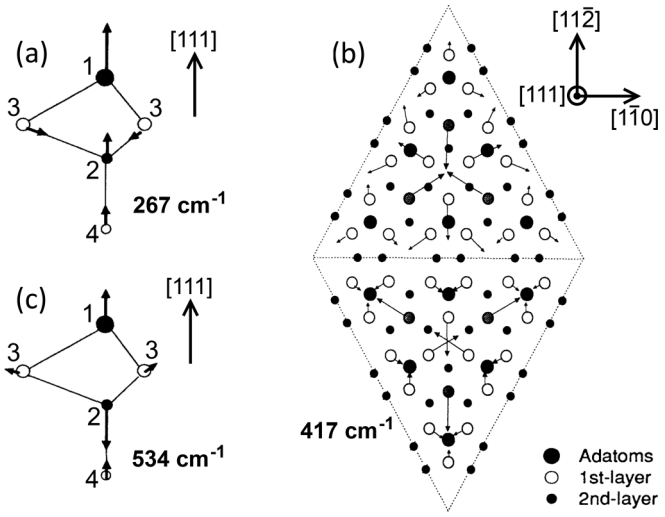

FIG. 6. Surface mode patterns: (a) local adatom vibration mode, (b) in-plane components of collective mode, (c) high-frequency split-off mode (adapted from Ref. [31]).

the mode pattern interpretation for some eigenfrequencies shows some discrepancies.

The most intuitive eigenmode of the DAS-reconstructed surface originates from localized normal-to-plane vibrations at adatomic sites. Figure 6(a) shows a realization which is dominated by in-phase vibrations of an adatom and atoms underneath along the [111] direction. In Ref. [31] its frequency was calculated in the range from 220 to 280 cm^{-1}, depending on whether the involved adatom is located at a corner- or an edge-center site. Therefore the experimentally observed peak at 250.9 cm^{-1} is attributed to this eigenmode. This assignment is additionally supported theoretically in Ref. [33], which also explains a calculated mode at $\sim$240 cm^{-1} in terms of a predominantly adatom feature. Furthermore, a HREELS study reports a broad structure (width beyond 50 cm^{-1}) centered at about 240 cm^{-1}, superimposed by a monotonously decaying background, which starts from the elastic line. This HREELS structure is assigned to a localized vibration mode of adatoms [35]. It should be noted that the observation of this vibration structure in HREELS until then had been impeded by a strong electronic continuum signal, caused by the metallic character of the Si(111)-(7×7) surface. In Ref. [35] this continuum was avoided by allowing small amounts of impurities on the surface, which did not destroy the local adatom reconstructions but suppressed both the high electronic continuum background and the broadening of the elastic reflected signal. In fact, regarding the adatom mode around 250 cm^{-1}, it is an advantage of Raman spectroscopy that this mode can be observed on a clean (7×7)-reconstructed Si(111) surface. Due to the most direct correlation of this localized adatomic vibration mode to the (7×7) DAS reconstruction, the appearance of this mode as a very narrow peak in the Raman spectrum is a key result of our investigation.

The observed mode at 420.0 cm^{-1} finds its correspondence in all calculations. It is a collective mode, involving the adatoms, as well as the first- and second-layer atoms. Figure 6(b) shows the in-plane components of the atomic displacement vectors, as calculated in Ref. [31], which reports

the eigenfrequency 417 cm^{-1}. Obviously, the vibrations of the faulted and the unfaulted half are out of phase, and a dominant contribution originates from the rest atoms in the first layer, an aspect which is also emphasized in Ref. [33]. It should be noted that nonvanishing normal-to-plane displacement vectors also occur in this mode, e.g., for the dimers and the adatoms. While this collective mode is also a primary fingerprint feature of the DAS-reconstructed surface, it did not appear in any spectroscopic study before. Just like the localized adatom vibration mode, its eigenfrequency is beyond the range which is accessible for HAS experiments.

Besides these two sharp and distinct peaks, a group of three closely spaced modes occurs in the frequency range from 110 to 140 cm^{-1}. They constitute the weakest peaks in the Raman spectrum and are clearly resolved only in the LT experiments at 40 K. In the calculation results of Refs. [33,34], the spectral weight in this frequency range is attributed to a massive in-plane wagging mode of the adatoms and the atoms directly underneath, with some involvement of first- and third-layer atoms as well. However, it should be noted that the power spectra from Ref. [31], shown in Fig. 5, primarily reveal a very strong contribution from the rest atoms in this frequency range. The calculated eigenfrequencies are ∼120 cm^{-1} [33], and 113 and 137 cm^{-1} [34].

All the modes in the frequency range above 100 cm^{-1}, discussed so far, concern specific dynamic deformation patterns of the reconstructed (7×7) unit cell. In addition, there also exist low-frequency acoustic modes in which the (7×7) cell moves as a whole, denoted as Rayleigh waves (RWs). In the mode interpretation of Ref. [33] the lowest calculated mode frequency at 60 cm^{-1} corresponds to a rigid-body in-plane translation oscillation and a second mode at 80 cm^{-1} to a rigid-body rotation vibration of the adatoms and atoms in the first two layers. Reference [34] also identifies distinctive RWs in the low-frequency range approximately between 60 and 100 cm^{-1}. These theoretical results are in good agreement with experimental HAS measurements as well, which show several backfolded Rayleigh modes, the first one centered at 61 cm^{-1} [36]. Therefore the observed peak at 62.5 cm^{-1} in the Raman spectra is attributed to these Rayleigh modes at the zone boundaries folded back to the BZ center at Γ.

The disappearance upon aging of all the surface Raman peaks, including the Rayleigh mode, underscores the strong impact of the applied gas-exposure procedure.

For the sake of completeness, it should be mentioned that all calculations consistently predict an additional mode, positioned between 533 and 600 cm^{-1}, dependent on the calculation method. This mode is denoted as a high-frequency split-off mode, whose mode pattern [shown in Fig. 6(c)] is derived from the 240-cm^{-1} mode [Fig. 6(a)] by inverting the vibration phase of atoms 2 and 3. Thus the backbone bond between atoms 2 and 4 is compressed, which strongly increases the mode stiffness. This mode was experimentally observed at 570 cm^{-1} by HREELS [35]. In our measurements, it could not be detected. This may be due to a very weak Raman activity, and possibly also due to its superposition by the high-energy tail of the very strong bulk LTO(Γ) phonon peak.

Finally, the polarization dependence of the Raman peaks is discussed in terms of the symmetry of the various elongation patterns. When the Si(111)-(7×7) surface with its C_{3v} symmetry is considered within the slab model with 151 movable atoms, it gives rise to 41 eigenmodes transforming according to A_1, 110 according to A_2, and 151 according to E [33]. In Ref. [33], it is pointed out that the main spectral features consist of a superposition of contributions with different symmetries.

The 240 cm^{-1} feature can be associated with peaks of all three possible symmetries of C_{3v}, i.e., A_1, A_2, and E, while the high-frequency split-off peak is composed of three peaks of A_1 and E symmetries. Because the Raman active modes A_1 and E have mode-specific nonvanishing Raman tensor elements, the polarization dependence of each peak intensity in the Raman spectrum gives information about the symmetry of the dominant scattering contribution.

As shown in Table I, the local adatom vibration at 250.9 cm^{-1} and the collective mode at 420.0 cm^{-1} essentially appear in perpendicular polarization configuration, which indicates that the Raman scattering process predominantly relies on their E-symmetry component. In contrast, the Rayleigh wave at 62.5 cm^{-1} and the wagging mode at 136.1 cm^{-1} show up mainly for parallel polarizations. Thus their scattering is primarily attributed to their A_1-symmetry contribution. The remaining Raman peaks, located at 115.3 and 130.0 cm^{-1}, originating also from wagging modes, are observed in both polarization configurations. Therefore we conclude that their scattering involves the A_1- as well as the E-symmetry component.

V. SUMMARY

We performed *in situ* polarized Raman spectroscopy experiments on a flash-cleaned (7×7)-reconstructed Si(111) surface. Six surface phonon modes were observed with frequency eigenvalues in the range between 62.5 and 420.0 cm^{-1}. These frequencies are in good agreement with results from molecular dynamics calculations, which yield for this complex surface a very high number of possible vibrations, but only about six to eight dominating frequency ranges. Thus our Raman peaks are explained in terms of the calculated eigenmodes with specific atomic site elongation patterns. The most relevant ones are localized adatom vibrations at 250.9 cm^{-1}, and collective vibrations of the adatoms and the first- and second-layer atoms at 420.0 cm^{-1}, because these modes are the most direct spectroscopic fingerprints of the (7×7) reconstruction. Furthermore, the Raman spectra show in-plane wagging vibrations in the range from 110 to 140 cm^{-1} and the acoustic Rayleigh wave, backfolded to the Brillouin zone center, at 62.5 cm^{-1}. Our observed surface mode frequencies agree very well with data of complementary experimental methods, where available. For the localized adatom vibration mode, the Raman peak allows a closer frequency specification, as compared with the reported results from electron energy-loss spectroscopy, while the Rayleigh mode frequency coincides with data from helium atom scattering. Moreover, the surface phonons show a mode-specific polarization dependence: some of them appear only for parallel polarization of the incident and scattered light, others for perpendicular polarization or for both configurations. From this polarization dependence the dominant symmetry component in the scattering process (A_1 or E symmetry) was deduced for each mode.

ACKNOWLEDGMENTS

We gratefully acknowledge financial support from the Deutsche Forschungsgemeinschaft in the research units FOR 1162, Project GE 1855/10-2, and FOR 1700, Project ES 127/12-1, and by the EFRE, Project 20072013 2/41, by the Senatsverwaltung für Wirtschaft, Technologie und Forschung des Landes Berlin.

[1] R. E. Schlier and H. E. Farnsworth, J. Chem. Phys. **30**, 917 (1959).

[2] W. Mönch, *Semiconductor Surfaces and Interfaces* (Springer, New York, 2001).

[3] F. Bechstedt, *Principles of Surface Physics* (Springer, New York, 2003).

[4] G. Binnig, H. Rohrer, C. Gerber, and E. Weibel, Phys. Rev. Lett. **50**, 120 (1983).

[5] K. Takayanagi, Y. Tanishiro, S. Takahashi, and M. Takahashi, Surf. Sci. **164**, 367 (1985).

[6] H. Huang, S. Y. Tong, W. E. Packard, and M. B. Webb, Phys. Lett. A **130**, 166 (1988).

[7] R. M. Tromp, R. J. Hamers, and J. E. Demuth, Phys. Rev. B **34**, 1388 (1986).

[8] E. Bengu, R. Plass, L. D. Marks, T. Ichihashi, P. M. Ajayan, and S. Iijima, Phys. Rev. Lett. **77**, 4226 (1996).

[9] P. Mårtensson, A. Cricenti, L. S. O. Johansson, and G. V. Hansson, Phys. Rev. B **34**, 3015 (1986).

[10] J. M. Nicholls and B. Reihl, Phys. Rev. B **36**, 8071 (1987).

[11] R. I. G. Uhrberg, T. Kaurila, and Y.-C. Chao, Phys. Rev. B **58**, R1730 (1998).

[12] I. K. Robinson, W. K. Waskiewicz, P. H. Fuoss, J. B. Stark, and P. A. Bennett, Phys. Rev. B **33**, 7013 (1986).

[13] G.-X. Qian and D. J. Chadi, Phys. Rev. B **35**, 1288 (1987).

[14] K. D. Brommer, M. Needels, B. E. Larson, and J. D. Joannopoulos, Phys. Rev. Lett. **68**, 1355 (1992).

[15] I. Štich, M. C. Payne, R. D. King-Smith, J.-S. Lin, and L. J. Clarke, Phys. Rev. Lett. **68**, 1351 (1992).

[16] *Light Scattering in Solids VIII: Fullerenes, Semiconductor Surfaces, Coherent Phonons*, edited by M. Cardona and G. Güntherodt (Springer, New York, 2000), Vol. 76.

[17] N. Esser, Appl. Phys. A **69**, 507 (1999).

[18] H. Ibach and D. L. Mills, *Electron Energy Loss Spectroscopy and Surface Vibrations* (Academic Press, New York, 1982).

[19] H. Nienhaus and W. Mönch, Surf. Sci. Lett. **328**, L561 (1995).

[20] H. Nienhaus, Phys. Rev. B **56**, 13194 (1997).

[21] G. Benedek and J. Peter Toennies, Surf. Sci. **299–300**, 587 (1994).

[22] M. Buongiorno Nardelli, D. Cvetko, V. De Renzi, L. Floreano, A. Morgante, M. Peloi, and F. Tommasini, Phys. Rev. B **52**, 16720 (1995).

[23] K. Hinrichs, A. Schierhorn, P. Haier, N. Esser, W. Richter, and J. Sahm, Phys. Rev. Lett. **79**, 1094 (1997).

[24] N. Esser, K. Hinrichs, J. R. Power, and W. Richter, Surf. Sci. **427–428**, 44 (1999).

[25] K. Fleischer, S. Chandola, N. Esser, W. Richter, and J. F. McGilp, Phys. Rev. B **76**, 205406 (2007).

[26] E. Speiser, S. Chandola, K. Hinrichs, M. Gensch, C. Cobet, S. Wippermann, W. G. Schmidt, F. Bechstedt, W. Richter, K. Fleischer, J. F. McGilp, and N. Esser, Phys. Status Solidi B **247**, 2033 (2010).

[27] J. Räthel, E. Speiser, N. Esser, U. Bass, S. Meyer, J. Schäfer, and J. Geurts, Phys. Rev. B **86**, 035312 (2012).

[28] V. Wagner, J. Wagner, S. Gundel, L. Hansen, and J. Geurts, Phys. Rev. Lett. **89**, 166103 (2002).

[29] *Light Scattering in Solids II: Basic Concepts and Instrumentation*, edited by M. Cardona and G. Güntherodt (Springer, New York, 1982), Vol. 50.

[30] K. L. Kostov, S. Polzin, S. K. Saha, O. Brovko, V. Stepanyuk, and W. Widdra, Phys. Rev. B **87**, 235416 (2013).

[31] J. Kim, M.-L. Yeh, F. S. Khan, and J. W. Wilkins, Phys. Rev. B **52**, 14709 (1995).

[32] I. Štich, K. Terakura, and B. E. Larson, Phys. Rev. Lett. **74**, 4491 (1995).

[33] I. Štich, J. Kohanoff, and K. Terakura, Phys. Rev. B **54**, 2642 (1996).

[34] L. Liu, C. S. Jayanthi, and S.-Y. Wu, Phys. Rev. B **68**, 201301(R) (2003).

[35] W. Daum, H. Ibach, and J. E. Müller, Phys. Rev. Lett. **59**, 1593 (1987).

[36] G. Lange, J. P. Toennies, P. Ruggerone, and G. Benedek, Europhys. Lett. **41**, 647 (1998).

[37] I.-S. Hwang, M.-S. Ho, and T.-T. Tsong, J. Phys. Chem. Solids **62**, 1655 (2001).

[38] R. Loudon, Adv. Phys. **13**, 423 (1964).

[39] M. Tinkham, *Group Theory and Quantum Mechanics* (McGraw-Hill Book Company, New York, 1964).

[40] T. C. Damen, S. P. S. Porto, and B. Tell, Phys. Rev. **142**, 570 (1966).

[41] P. A. Temple and C. E. Hathaway, Phys. Rev. B **7**, 3685 (1973).

[42] K. Uchinokura, T. Sekine, and E. Matsuura, J. Phys. Chem. Solids **35**, 171 (1974).

[43] A. Zwick and R. Carles, Phys. Rev. B **48**, 6024 (1993).

[44] A. Compaan, M. C. Lee, and G. J. Trott, Phys. Rev. B **32**, 6731 (1985).